ELSEVIER

Polymer 43 (2002) 6147–6157

polymer

www.elsevier.com/locate/polymer

Structural characterization and transport properties of organically modified montmorillonite/polyurethane nanocomposites

Mariarosaria Tortora[a,*], Giuliana Gorrasi[a], Vittoria Vittoria[a], Giancarlo Galli[b], Stefano Ritrovati[b], Emo Chiellini[b]

[a]*Dipartimento di Ingegneria Chimica e Alimentare, Università di Salerno, Via Ponte Don Melillo, 84084 Fisciano, Italy*
[b]*Dipartimento di Chimica e Chimica Industriale, Università di Pisa, Via Risorgimento 35, 56126 Pisa, Italy*

Received 15 May 2002; received in revised form 30 July 2002; accepted 14 August 2002

Abstract

Samples of polyurethane and organically modified montmorillonite (OMont) were prepared, covering a wide range of inorganic composition, up to 40 wt%. They were obtained by a three step process using diphenylmethane diisocyanate, poly(ε-caprolactone), di(ethylene glycol) and poly(ε-caprolactone)–OMont (NPCL) nanocomposites. The NPCL nanocomposites were used as soft segments for a partial replacement of the di(ethylene glycol) in the hard-segment of the polymeric chains.

The X-ray analysis showed that exfoliation occurred for low montmorillonite content, whereas for higher contents the intercalated clay rearranged to a minor extent. The mechanical and dynamic–mechanical analysis showed an improvement of the elastic modulus and yield stress, but a decrease of the stress and strain at breaking on increasing the clay content. Sorption and diffusion were measured for two different vapors, i.e. water vapor as hydrophilic permeant and dichloromethane as hydrophobic one. For both vapors the sorption did not drastically change on increasing the clay content. At variance the zero-concentration diffusion parameter (D_0) strongly decreased on increasing the inorganic content. The permeability, calculated as the product of the sorption (S) and the zero-concentration diffusion coefficient (D_0) showed a remarkable decrease up to 20% of clay and a leveling off at higher contents. It was largely dominated by the diffusion parameter. © 2002 Published by Elsevier Science Ltd.

Keywords: Nanocomposites; Montmorillonite; Intercalation

1. Introduction

Polymer composites are composed of two or more constituent materials possessing complementary physical and chemical properties, that are expected to produce synergistic properties difficult to obtain separately from those of the individual components.

The composites having more than one solid phase with a dimension in the 1–20 nm range are referred to as nanocomposites [1–4]. Nanocomposites are a new class of materials showing better physical properties—such as thermal, mechanical and barrier properties—than conventional composites, because of the much stronger interfacial forces between the nanometer-sized domains.

The most common nanocomposites are composed of polymers and organically modified montmorillonite (OMont) [4]. Natural montmorillonite has a layered structure made up of disc shaped silicate layers with dimensions of approximately 100 nm in diameters, and 1 nm in thickness. Isomorphic substitution within the layers generates negative charges that are normally counterbalanced by cations residing in the interlayer galleries space [2,4]. Since montmorillonite is hydrophilic and lacks affinity with hydrophobic organic polymers, ion-exchange reactions of montmorillonite with various organic cations, such as alkylammonium cations, is needed in order to give a partial hydrophobic character to the originally hydrophilic silicate surfaces. The organic cations lower the surface energy of silicate layers and enhance the miscibility between the silicate layers and the polymer matrix. The preparation of a polymer–OMont nanocomposite usually involves intercalation of a suitable monomer into swellable layer silicate host followed by polymerization and, possibly, exfoliation of the layered host into its nanoscale elements [5–9]. Alternatively, a melt-direct polymer intercalation

* Corresponding author. Fax: +39-89964057.
E-mail address: mrtortora@unisa.it (M. Tortora).

0032-3861/02/$ - see front matter © 2002 Published by Elsevier Science Ltd.
PII: S0032-3861(02)00556-6

using a conventional polymer extrusion process can be used [10–14]. Although a variety of polymers have been investigated as the continuous polymer phase in nanocomposites with dispersed OMont [5–14], polyurethanes (PUs) have comparatively received little attraction as the polymer matrix [15].

The physical properties of PUs are derived from their molecular structure as well as the supramolecular structure caused by interaction between the polymer chains. The segmental flexibility, the chain entanglement, the interchain forces and the cross-linking are all factors that influence the properties and determine the use of the end-products. As a matter of fact, PUs are used in a variety of applications, especially as thermoplastic elastomers [16–18]. The structures and properties of thermoplastic segmented PU had been studied by different research groups [19–21]. On a molecular basis, thermoplastic urethane elastomers may be described as linear block copolymers of the $(AB)_n$ type. One block of the polymer consists of a relatively long, flexible polyester or polyether diol. These blocks are usually termed the soft segments since they impart the elastomeric character to the polymer. The second block of the copolymer is commonly referred to as the hard-segment and is formed by the reaction of aromatic diisocyanates with low molecular diol or triol chain extender. The elastomeric properties of these block copolymers are generally attributed to the phase separation of the PU and polyol segments, whereby the hard PU domains serve as cross-links and filler particles in the matrix of the polyol segment. Both physical and chemical studies have shown that bulk properties depend on the nature and extent of phase separation [22–27]. The extent of compatibility between the segmented blocks of the PUs is of particular interest when the soft segments consist of polycaprolactone; in fact, polycaprolactone exhibits a unique ability to blend with a variety of polymers over a wide composition range and is truly compatible with different polymers [24–26].

The aim of this work was to prepare samples of PU–OMont nanocomposites (NPU) covering a wide range of montmorillonite compositions (up to 40 wt%), using poly(ε-caprolactone)–OMont nanocomposites (NPCL). The investigation of the effect of the percentage of montmorillonite, and the morphology of the manufacture, on the physical and transport properties of the nanocomposite were investigated.

2. Experimental

2.1. Materials

4,4′-Diphenylmethane diisocyanate (MDI), di(ethylene glycol) and poly(ε-caprolactone) diol ($M_n = 1250$, PCL) (Aldrich) were used as received. *N*, *N*-Dimethylformamide (DMF) (Carlo Erba) was distilled over CaH_2 under reduced pressure and stored over 4 Å molecular sieves. The synthesis and the properties of the poly(ε-caprolactone)/O-Mont nanocomposites used for the preparation of the PU nanocomposites were reported in a previous article [28].

2.2. Synthesis of PU/clay nanocomposite (NPU)

The weight percentage of montmorillonite in the NPU, determined by thermogravimetric analysis (TGA), is represented by Y in NPUY (e.g. NPU4 is a nanocomposite of PU with 4 wt% of montmorillonite). Segmented NPUs were synthesized by a three step process. The synthesis of NPU4 is reported as an example: 2.00 g (1.6×10^{-3} mol) of PCL and 0.518 g (2.1×10^{-3} mol) of MDI in 15 ml of DMF were mixed under nitrogen atmosphere for 2 h at 70 °C. Then, 0.0240 g (2.3×10^{-4} mol) of the chain extender di(ethylene glycol) was added and the system was stirred for 2 h. Subsequently, 1.00 g (1.0×10^{-4} mol) of NPCL nanocomposite was added to the mixture and the reaction was performed for an additional 2 h. The resulting NPU was poured in methanol, and the recovered solid was dried in vacuo.

2.3. Polymer recovery from NPU

Five milliliters of toluene (Carlo Erba) was added to 0.5 g of the synthesized NPU while stirring for 2 h at room temperature. Then, 10 ml of a 1% LiCl (Carlo Erba) solution in DMF was gradually added to the suspension. The mixture was stirred for 48 h to perform the reverse ion-exchange reaction, then the solution was centrifuged at 3500 rpm for 10 min. The supernatant liquid after centrifuge was poured in methanol and the resultant solid (EPU) was filtered and dried in vacuo.

2.4. Methods of investigation

FT-IR analysis was performed on KBr pellets with a Perkin Elmer 1600 spectrophotometer.

The ^1H NMR spectra of the nanocomposites and the polymers recovered from the nanocomposites were recorded at 25 °C with a Varian Gemini 200 spectrometer. Samples (40 mg) were dissolved in $CDCl_3$ (1 ml).

Molecular weights of the polymers were determined by gel permeation chromatography (GPC) in $CHCl_3$ using polystyrene standard for calibration.

X-ray diffraction measurements (XRD) were performed on powder samples with a Philips diffractometer (equipped with a continuous scan attachment and a proportional counter) with Ni-filtered Cu Kα radiation (1.541 Å).

Differential scanning calorimetry (DSC) were obtained with a DSC-30 under N_2 atmosphere at a heating rate of 20 °C/min.

TGA was carried out in a nitrogen atmosphere by means of a Mettler TC-10 thermobalance from 30 to 750 °C at a heating rate of 10 °C/min.

Films of the nanocomposites and the pure polymer were

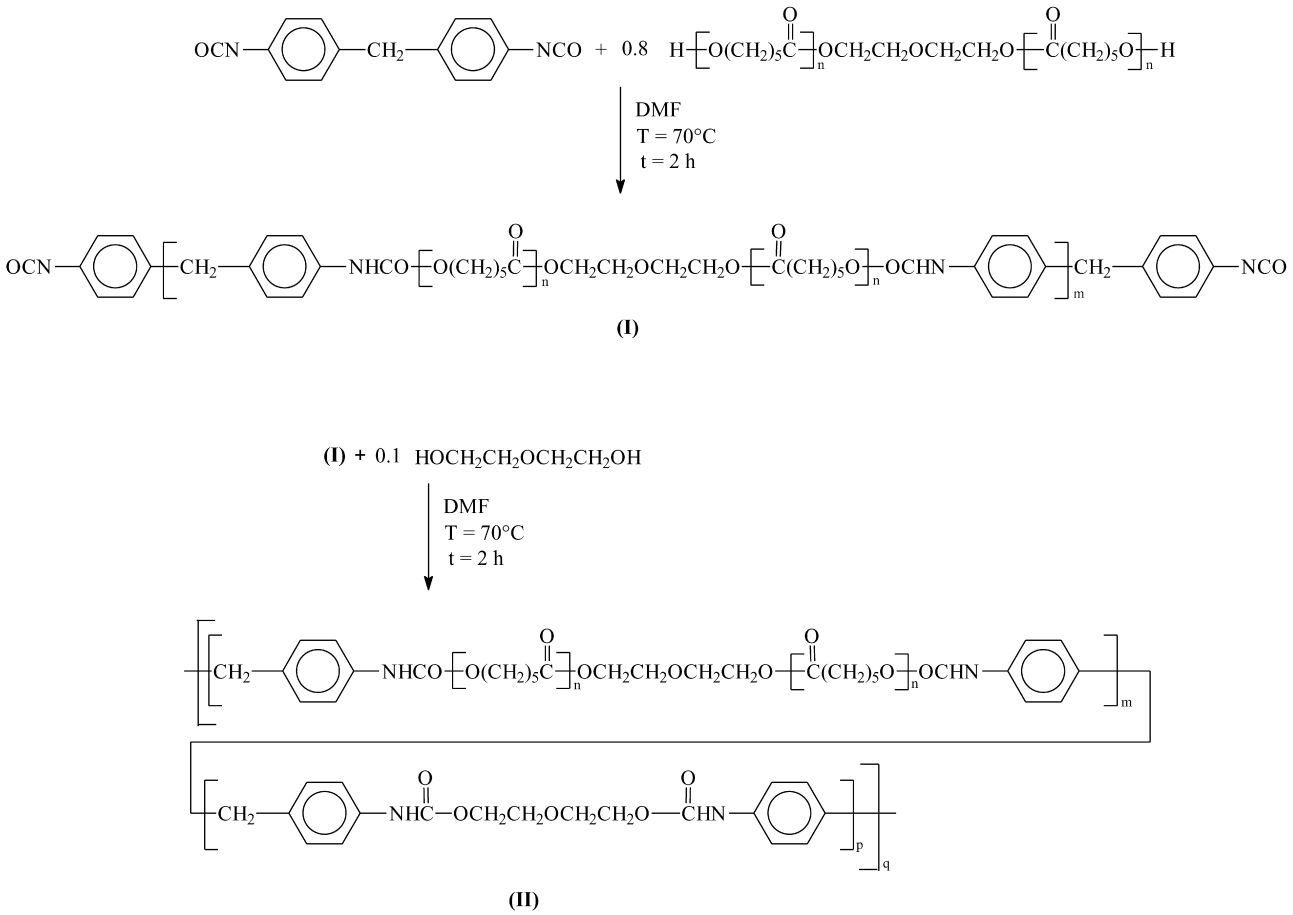

Scheme 1. Reaction pattern followed to obtain the PU segments.

obtained by molding the powders in a Carver Laboratory Press, at the temperature of 100 °C, followed by a quick quenching in a ice-water bath.

The mechanical properties of the samples were evaluated from stress–strain curves obtained using a dynamometric apparatus INSTRON 4301. The experiments were conducted at room temperature with the deformation rate of 2 mm/min. The initial length of the samples was 10 mm, the thickness was 0.1 mm. Elastic moduli were derived from the initial part of the stress–strain curves, giving to the sample a deformation of 0.1%.

The transport properties were measured by the microgravimetric method, using a quartz spring balance having an extension of 1.62 cm/mg. The permeants were dichloromethane and water vapor. Sorption was measured as a function of vapor activity $a = p/p_0$ where p is the actual pressure (in mm Hg) of the experiment, and p_0 the saturation pressure at 25 °C for dichloromethane (410 mm Hg) and at 30 °C for water (32 mm Hg).

Dynamic–mechanical properties were performed using a Polymer Laboratories Dynamic Mechanical Thermal Analyzer. The spectra were recorded in the tensile mode, obtaining the logarithm of the modulus E', and the loss factor, tan δ, at a frequency of 1 Hz, as a function of temperature. The heating rate was 5 °C/min in the range of −100 to 150 °C.

3. Results and discussion

3.1. Polymer synthesis

In Schemes 1 and 2, the synthesis and one simplified chemical structure of the NPUs are reported. As shown in Scheme 1, in the first step, an excess of diisocyanate reacted with the poly(ε-caprolactone) diol to form isocyanate-terminated urethane oligomers. In the second step, less than a stoichiometric amount of di(ethylene glycol) was used as a chain extender to produce PU. Then, as reported in Scheme 2, in the third step of the reaction a fixed number of moles of previously prepared nanocomposites poly(ε-caprolactone)/OMont (NPCL) was added leading to the eventual nanocomposites. It was possible to obtain NPU nanocomposites with a Mont content varying regularly from 0 to 40 wt%, using NPCLs nanocomposites based on different contents of OMont (for details on the synthesis of the NPCLs see Ref. [28]). As shown in Scheme 2, the NPCL nanocomposite represents the end-capping part of the polymer structure. In the prepared NPCLs, some PCL

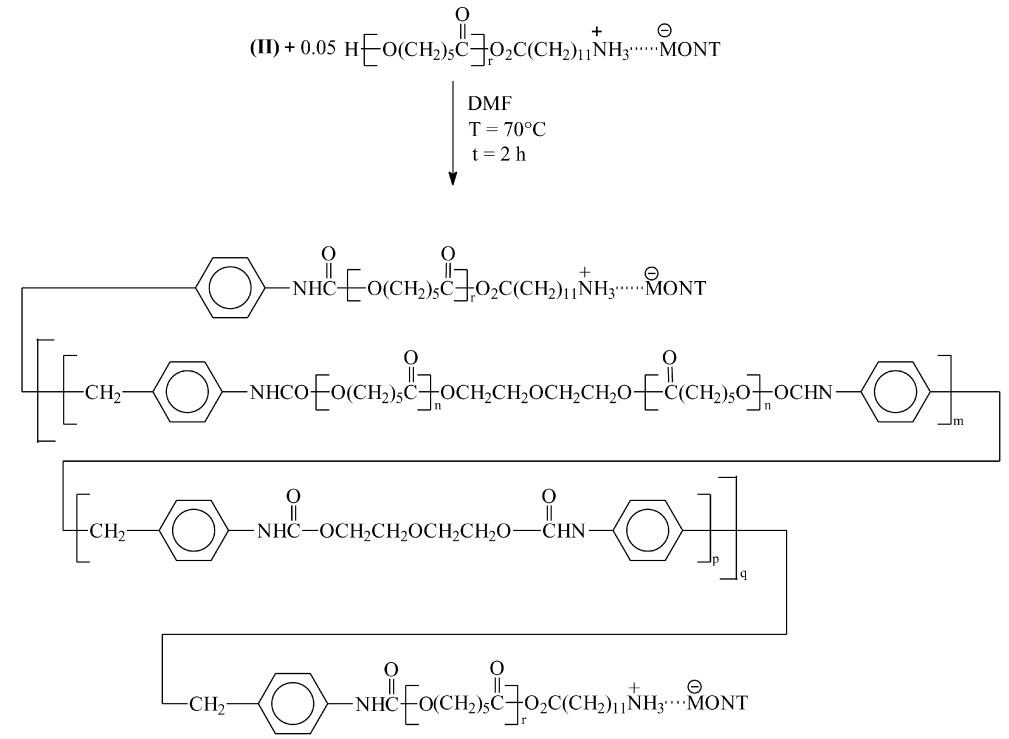

Scheme 2. One simplified chemical structure of the prepared NPUs.

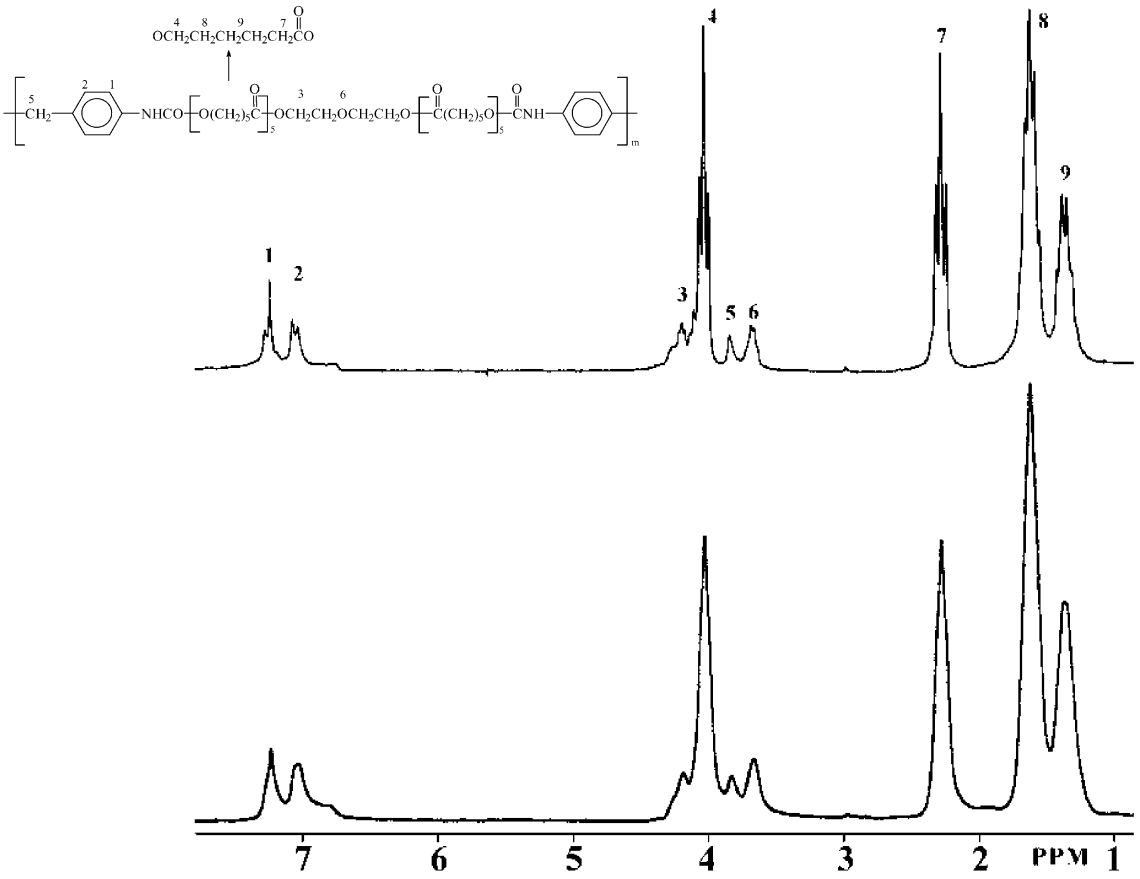

Fig. 1. ^{1}H NMR spectra of NPU4 (bottom) and EPU4 (top).

macromolecules may be physically, not chemically bonded to the Mont and, in this case, the terminal groups that react with (II) would be doubled. The obtained segmented NPUs are based on low hard-segment concentrations, in fact they contain PCL/Mont as a partial replacement of the di(ethylene glycol) in the hard-segment. The codes, the content of the Mont, evaluated by TGA, and the molecular weight of the recovered PU are reported in Table 1.

3.2. Structural characterization

The IR spectra can help confirm the synthesis of the urethane polymers, due to the presence of characteristic absorption bands. As a matter of fact the IR spectra of all the synthesized NPUs (not shown here) exhibited prominent absorptions at 1750 cm^{-1} due to the stretching of the C=O group; the 2940 and 2860 cm^{-1} peaks were due to the asymmetric and symmetric C–H stretching vibration. The peak at 3350 cm^{-1} was due to the N–H group hydrogen bonded urethane.

The molecular structure of the polymers recovered from the NPUs was confirmed by ^1H NMR spectroscopy. In Fig. 1 the ^1H NMR spectra of NPU4 and the corresponding PU extracted from NPU4 (EPU4), are reported as typical examples. The signal broadening seen in NPU4 was due to the attachment of polymer chains to the silicate layers, as in fact it disappeared in the spectrum of EPU4.

The X-ray diffractograms of OMont, NPU0, NPU4, NPU20 and NPU40 are shown in Fig. 2. In the OMont spectrum (a) a diffraction peak at $2\theta = 6.2°$, corresponding to a basal spacing of the clay platelets of 14 Å, was present. In the patterns of NPU4 (c) the peak at $2\theta = 6.2°$, was totally absent, thus suggesting the exfoliation of the clay platelets in the polymeric matrix. A different situation was observed in the XRD patterns of NPU20 and NPU40, where a peak was visible at $2\theta = 5.6°$ corresponding to a basal spacing of 15 Å, and its intensity increased on increasing the clay content in the NPU. The presence of these peaks in the NPU20 (d) and NPU40 (e) spectra suggested that the layer structure of the intercalated clay rearranged to a minor extent. In all the spectra of each NPU two strong peaks (not shown in Fig. 2) were detected at $2\theta = 21.3$ and 23.7° due to the crystalline structure of PCL present in the PUs.

It can be concluded that the reaction scheme adopted gave rise to nanocomposites in which the silicate layers were either delaminated (or exfoliated) or ordered in an intercalated structure. When the clay weight fraction is very high (NPU20 and NPU40), the intercalated structure was essentially a well ordered multilayer. In the delaminated structure, which was formed in NPU4, the individual silicate platelets were predominantly dispersed in the polymer matrix.

Table 1
Composition of the NPUs synthesized and molecular weights of the respective extracted EPUs

Nanocomposite	OMont content[a] (wt%)	M_n[b] (g/mol)	M_w[b] (g/mol)
NPU0	0	22,000	51,000
NPU4	4	12,000	33,000
NPU20	20	12,000	40,000
NPU40	40	13,000	53,000

[a] Determined by TGA.
[b] Determined by GPC, on EPU recovered from the NPU nanocomposite.

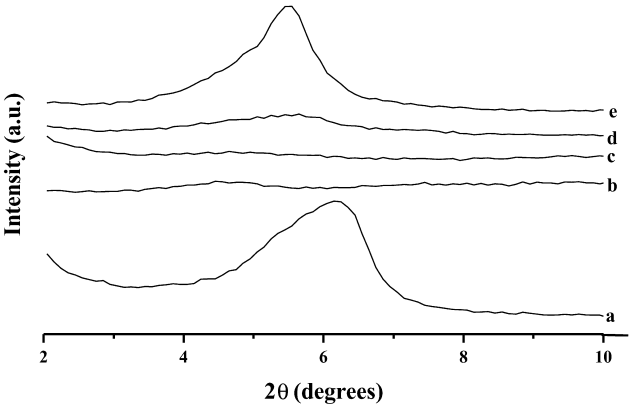

Fig. 2. Wide-angle X-ray diffractograms of (a) OMont, (b) NPU0, (c) NPU4, (d) NPU20 and (e) NPU40.

3.3. Physical properties

3.3.1. Differential scanning calorimetry

The DCS curves of samples NPU0, NPU4, NPU20 and NPU40, not reported, are conventional and display the melting process of the poly(ε-caprolactone) present in the NPU. In Table 2 all the thermal data are reported. From the melting temperature values (ranging between 48 and 54 °C), it is evident that poly(ε-caprolactone), either when used pure or clay-polymerized, crystallizes in the PU samples. The ability of poly(ε-caprolactone) to crystallize within the PU sample was always found for poly-(ε-caprolactone) of molecular weight higher than 3100 [24]. The melting enthalpy strongly decreases on increasing the clay content, going from 26 J/g for sample NPU0, to 18 J/g for sample NPU20 and 15 J/g for sample NPU40 (Table 2). Very peculiar, and not easily explicable the behavior of NPU4, which shows a much higher melting enthalpy value of 40 J/g. The glass transition temperatures range between −25 and −33 °C. The inflection point temperature decreases on increasing the clay content in the

Table 2
Thermal properties of the synthesized NPUs

Nanocomposite	T_g (°C)	T_m (°C)	ΔH (J/g)[a]
NPU0	−31	48	26
NPU4	−25	52	40
NPU20	−28	50	18
NPU40	−33	54	15

[a] Normalized to the content of PU.

polymer, showing the influence of the inorganic component on the amorphous phase, too. The amorphous state environment is clearly influenced by the concentration of soft and hard-segments and, in our case, also by the clay content. However, the study of the glass transition, of either the soft or the hard-segments, is better performed by dynamic–mechanical analysis, and will be presented and discussed in the following.

3.3.2. Dynamic–mechanical properties

The structure, concentration and organization of the hard-segments, and their interaction with the soft segments, have a dominant influence on the physical and mechanical properties of the urethane polymers. For this reason we performed a dynamic–mechanical analysis on the clay-composite PUs, in which the soft part contains a progressively increasing clay content.

In Fig. 3, the changes of the logarithm of the elastic modulus E' and the loss factor (tan δ) with the temperature

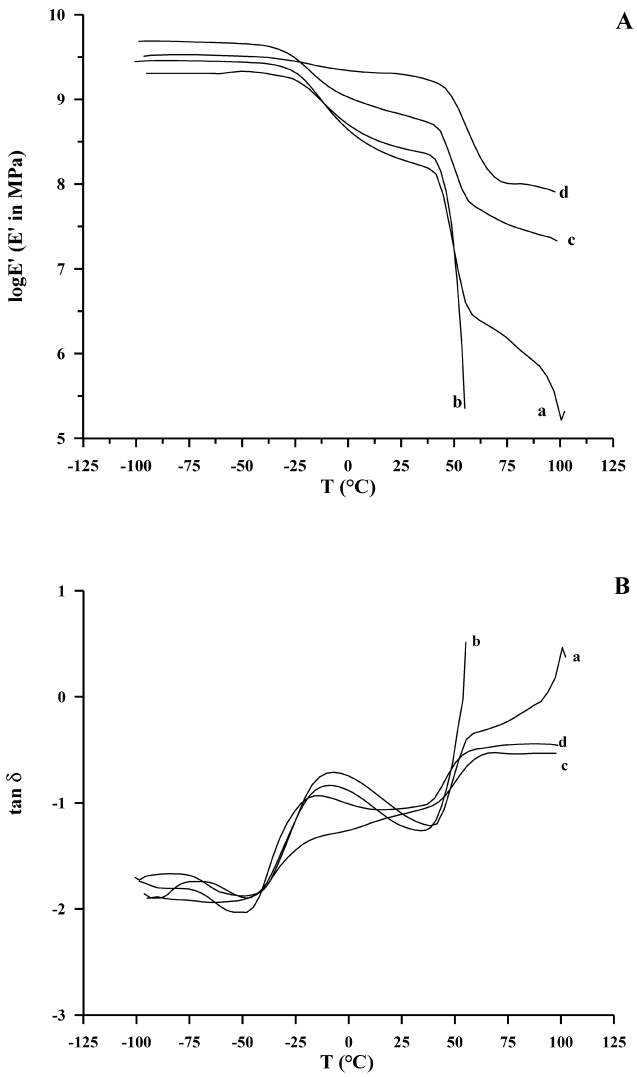

Fig. 3. log E' (E' in MPa) (A), and tan δ (B) as function of temperature for NPU0 (a), NPU4 (b), NPU20 (c) and NPU40 (d).

are reported, for samples NPU0 (a), NPU4 (b), NPU20 (c), and NPU40 (d).

For the NPU0 polymer we observe a slightly decreasing linear behavior of the elastic modulus up to −28 °C, followed by a sharp drop, associable to the glass transition of the polymer. The drop decreases the elastic modulus by more than one and half orders of magnitude. A second, very steep drop, ending with the loss of mechanical consistence, is observable around 50 °C. Therefore, in the case of the pure polymer, free of inorganic component, the disordering of the crystalline domains produces a strong modulus reduction above the melting. The modulus definitively collapses at 100 °C, where the glass transition of the hard domains can be located.

As for the loss factor, tan δ, we observe a broad peak, of very low intensity, between −95 and −70 °C. This peak was already reported in urethane polymers as a secondary relaxation, becoming more prominent as the concentration of hard-segments was increased [29]. The analysis of this transition in urethane polymers with different lengths of hard-segments, suggested that it could arise from the disruption of the associations between hard and soft segments [25].

At higher temperature, a more intense peak, due to the mobilization of the amorphous soft domains, appears in the correspondence of the elastic modulus drop, at about −6.5 °C. This suggests that this peak is associated to the main glass transition of the system, due to the amorphous domains.

As shown in the figure, a further strong dissipation occurs in correspondence of the melting of the crystalline phase, where the steep drop in the elastic modulus is evident. As noted before, after melting the sample shows a much lower modulus up to the hard domains transition, occurring after 100 °C.

The behavior of sample NPU4 is very similar to that of the pure PU, although the drop of the elastic modulus in the transition region of the soft segments is reduced, changing less than one order of magnitude. Also in this case, the melting of the crystalline phase at about 50 °C determines a second drop in the modulus. However, in the case of sample NPU4, containing 4% of clay, the melting of the crystalline phase results in the complete collapse of the modulus and the loss of mechanical consistence of the sample. In this case we must hypothesize that the hard domains transition occurs in the same temperature range as the melting of the crystalline phase. Probably very few hard domains are formed in this sample, and this can explain the low transition temperature. As for the loss factor, tan δ, we observe that the peak at low temperature, although showing a similar intensity, is shifted to higher temperature. At variance the position of the maximum of the main peak occurs at a slightly lower temperature (−10 °C), and its intensity is reduced, due to the less extent of amorphous phase, as shown by DSC.

The behavior of samples NPU20 and NPU40 is very

interesting. We note that the drop of the elastic modulus of sample NPU20, due to the glass transition of the soft segments, is much smaller than that of the pure polymer, determining a much higher modulus in the whole interval up to the melting, occurring at about 50 °C. Moreover, the melting of the crystalline phase does not determine the loss of consistence of the sample and, after the drop in the melting region, the modulus shows a still high value up to temperatures well above the melting point. This behavior is even more marked in sample NPU40, in which indeed no drop in E' is observed in the glass transition range. Therefore, in the temperature range up to the melting the modulus is high and typical of a glassy polymer. In the melting region only a reduced drop of modulus is observable without the loss of mechanical consistence, up to the highest investigated temperature. This result is consistent with the formation of an entangled and interconnected network of hard domains at high clay contents, which survives the melting of the crystals, and preserves the mechanical consistence of the melted sample up to very high temperatures. The thermally reversible network structure provides for the apparent cross-linked nature of samples NPU20 and NPU40 after melting of the crystalline phase.

The transition at low temperature, as evident by the tan δ behavior, was much reduced in sample NPU20, whereas in sample NPU40 completely disappeared, suggesting that the presence of clay in the poly(ε-caprolactone) progressively reduces and finally eliminates the interactions between hard and soft segments. Moreover, we notice that the intensity and the temperature of the main transition peak decrease on increasing the clay content in samples NPU20 and NPU40. In sample NPU40, with the highest clay content a continuous transition extending up to the melting is observable after the main transition peak, indicating a broad distribution of molecular mobility. In other words, there is not a distribution of molecular mobility centered at a definite temperature, but a continuous distribution of molecules that are mobilized at increasing temperature, up to the hard domains transition, well above the melting range. The decrease of the peak intensity can be associated to a decrease of the relative amount of amorphous phase, undergoing the transition from the glass to the rubbery state. Although the amorphous fraction increases (as shown by the melting enthalpy decrease) on increasing the clay content the total quantity of poly(ε-caprolactone) decreases and therefore so does the glass transition intensity.

3.3.3. Stress–strain behavior

The engineering load versus elongation curves for samples NPU0 (a), NPU4 (b), and NPU20 (c) are shown in Fig. 4. Sample NPU40 resulted very brittle, breaking just after the yield point: therefore it was only possible to measure its elastic modulus.

The drawing curve of sample NPU0 is conventional with upper and lower yield points describing the neck formation

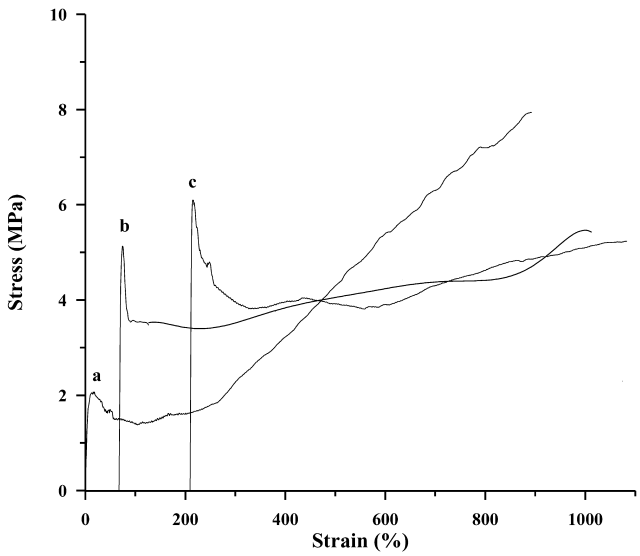

Fig. 4. Stress–strain plots for NPU0 (a), NPU4 (b) and NPU20 (c). The different curves are shifted on the *x*-axis, for clarity.

and the subsequent transformation into an oriented structure. Upper and lower yield stresses are restricted in a sharp deformation range that, at a macroscopic level, characterizes the appearance of a neck. The local deformation drastically increases in the neck producing a significant reduction in the local cross-section: this effect induces a stress-concentration that stabilizes the neck and the axial drawing takes place through the neck propagating to the whole sample. This stage of the drawing process occurs at constant load, and therefore the plateau region of the stress identifies the deformation range characterized by the neck propagation. When the neck propagated to the whole sample, the stress increases producing the orientation of the system shown by the large strain-hardening which increases the stress up to the fracture. For sample NPU0 the horizontal part of the curve, after the yield drop, ends before 300% of elongation; afterwards a steep increase of stress on elongation, and the breaking point at about 850% of elongation are observable.

Samples NPU4 and NPU20 show a much more pronounced yield and post-yield drop than the neat sample. The value of the stress at the yield point increases on increasing the clay content as well as the elastic modulus. At variance, a much lower strain-hardening is observable for both the hybrid samples, and they break at a consistently lower stress, although the breaking strain is very similar to the parent sample. This result indicates a different morphology of the hybrid materials, which is less available to be fragmented and oriented. As a matter of fact, the much more accentuated strain-hardening of sample NPU0 indicates a higher orientation of the neat sample and also a higher breaking stress. Morphological investigations are needed to verify this hypothesis, and they are in progress.

All the mechanical parameters, derived from the stress–strain curves are reported in Table 3. It is evident

Table 3
The mechanical properties evaluated from the stress–strain curves relative to all the samples

Nanocomposite	E (MPa)	σ_y (MPa)	σ_b (MPa)	ε_b (%)	Energy at break point (J)
PUB	50	1.48	7.82	1072	0.400
NPU4	160	3.80	5.50	960	0.127
NPU20	280	5.20	5.30	778	0.282
NPU40	270	–	–	–	–

that even the presence of a small amount of OMont largely improves the stiffness of the blends, as can be seen from the values of the elastic moduli. As a matter of fact, 4% of OMont is enough to triplicate this parameter, from 50 MPa of sample NPU0 to 160 MPa of sample NPU4. Still higher the elastic modulus of sample NPU20 with 20% of OMont, that is 280 MPa, whereas no further increase is seen for the highest content of clay, that is sample NPU40 with 40% of OMont. The toughness and the drawability appear to be reduced in the hybrid samples, as evident from either the stress at break, or the energy at break point (J), whereas the percentage of elongation at break is not consistently reduced.

Finally, we must observe that the mechanical parameters, such as elastic modulus and stress at the yield point, are better than those of the pure PU sample already with 4% of OMont content, and are not really much improved going from 4 to 20 and 40%. Such results allow to hypothesize that the lower is the OMont percentage, the better is the adhesion between the two phases, with consequently highly improved mechanical parameters, at least for what concerns elastic modulus and yield stress.

3.3.4. Transport properties

A nanocomposite is a multiphase system in which the coexistence of phases with different permeabilities can cause complex transport phenomena. In fact, the organophilic montmorillonite gives rise to superficial adsorption and to specific interactions with the solvents. In turn, the polymer phase itself can be considered as a two-phase crystalline–amorphous system, the crystalline regions being generally impermeable to the penetrant molecules.

The presence of the montmorillonite layers may be expected to cause a decrease in permeability due to a more tortuous path for the diffusing molecules that must bypass impenetrable platelets. Therefore, to determine how the content of montmorillonite in a hybrid composite would affect the sorption and diffusion of the nanocomposites, the transport properties were investigated for all the samples prepared using water vapor as a hydrophilic solvent and dichloromethane as a hydrophobic one. In fact, in this way the barrier and the physical properties of a multiphase system composed of hydrophilic regions (OMont) and dispersed hydrophobic phase (PU) could be studied.

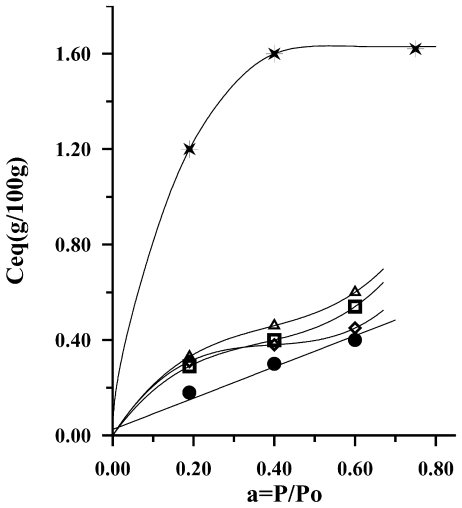

Fig. 5. Equilibrium concentration of water vapor, C_{eq} (g/100 g), as a function of activity $a = p/p_0$ for samples OMont (★), NPU0 (●), NPU4 (□), NPU20 (△), NPU40 (◇).

3.3.4.1. Water vapor. In Fig. 5 the equilibrium concentration, C_{eq} (g/100 g) of water vapor as a function of the vapor activity, $a = p/p_0$, for all the NPUs and for the OMont, measured at 30 °C is shown. The sorption curve of water vapor for OMont follows the Langmuir sorption isotherm in which the sorption of solvent molecules occurs on specific sites; therefore when all the sites are saturated a plateau is reached. The sorption of NPU0 sample shows a linear dependence of equilibrium concentration on activity, and therefore an ideal behavior. As expected, at each activity, the sorption of OMont is greater than that of the NPU0, due to its higher hydrophilicity.

The sorption curves of the other NPUs show the dual-sorption shape, that is a downward concavity, an inflection point and an upward curvature. In the first zone the sorption of solvent molecules on specific sites due to interacting groups is the prevailing mechanism. We can infer that this type of sorption is due to the presence of the clay in the polymers. At higher activities, the plasticization of the polymeric matrix determines a more than linear increase of vapor concentration, and we observe a transition in the curve from a dual type to a Flory–Huggins behavior. It can be observed that at low activities ($a \leq 0.2$) the equilibrium concentration increases on increasing OMont content in the composites, as expected for the higher hydrophilicity of the montmorillonite. The sorption parameter (S), can be obtained reporting the equilibrium concentration (C_{eq}) of the permeant vapor as a function of the partial pressure (p) [30]. It is defined as:

$$S = \mathrm{d}(C_{eq})/\mathrm{d}p \quad (1)$$

All the S parameters, derived at low pressures according to Eq. (1), are reported in Table 4.

Reporting the concentration of sorbed vapor as a function of the square root of time, in the case of Fickian behavior, it is possible to derive for each vapor activity a mean diffusion

Table 4
Zero-concentration diffusion coefficients, D_0 (cm^2/s), and sorption coefficients S (g/100 g mm Hg) of water vapor at $a \leq 0.2$ for all the analyzed samples

Sample	S[a] (g/100 g mm Hg)	$D_0 \times 10^7$ (cm^2/s)
PU	0.029	1.20
NPU4	0.047	0.444
NPU20	0.050	0.0734
NPU40	0.050	0.0654

[a] Evaluated as the slope of the straight line at $a \leq 0.2$ in the C_{eq} versus p (in mm Hg) curve.

coefficient, D, using the following equation [31,32]

$$C_t/C_{eq} = 4d(Dt/\pi)^{1/2} \quad (2)$$

where d is the thickness of the sample, C_t is the penetrant concentration at the time t, and C_{eq} is the penetrant concentration at the equilibrium value. The diffusion parameter is not constant at each vapor activity, but increases with increasing vapor concentration. For many vapor penetrant pairs diffusion depends on the equilibrium concentration, C_{eq} (g/100 g) at a given activity, and generally this dependence can be expressed as [33]

$$D = D_0 \exp(\gamma C_{eq}) \quad (3)$$

where D_0 (cm^2/s) is the zero-concentration diffusion coefficient related to the fractional free volume and to the microstructure of the polymer; γ is the concentration coefficient, which depends on the fractional free volume and the effectiveness of the penetrant to plasticize the matrix, too.

In Fig. 6 we report the diffusion coefficient evaluated at each vapor pressure, as a function of the concentration of water vapor absorbed by the samples. A linear dependence of D on the C_{eq}, of water sorbed, in all the investigated range, allows the determination of the thermodynamic parameter D_0 through extrapolation to zero penetrant concentration.

The numerical values of D_0 are reported in Table 4. The decrease of the D_0 values with increasing OMont content in the NPUs can be attributed to a more tortuous diffusion path which the water molecules must cover as a consequence of a greater presence of the OMont platelets.

The permeability of the samples to the vapors is calculated as the product of sorption and diffusion:

$$P = D_0 S \quad (4)$$

It represents the thermodynamic parameter P, considering that we use the zero-concentration diffusion coefficient and the derivative of the equilibrium concentration versus pressure at low vapor pressures. Although it is not a technological parameter, that can be only determined in the use conditions of the material, it is of fundamental importance with the purpose to correlate the physical properties to the structure of the samples.

In Fig. 7 the logarithm of P to water vapor, as a function of OMont content in NPUs is reported. The permeability decreases linearly up to 20% of OMont, then a plateau value is reached. Since D_0 and S of the NPUs have opposite trends it is concluded that the permeability behavior, at low activities, is largely dominated by the diffusion phenomenon.

3.3.4.2. Dichloromethane vapor. Fig. 8 shows the equilibrium concentration of sorbed dichloromethane, as a function of vapor activity, for the NPUs and OMont at 25 °C. The behavior of the sorption curve of dichloromethane vapor OMont is similar to that shown in Fig. 5 for the same sample when exposed to the water vapor.

The isotherms relative to samples NPU0 and NPU4 display a first range up to $a \leq 0.3$ in which the systems follow an ideal behavior: the sorption is linear with the vapor partial pressure. For higher vapor activities the

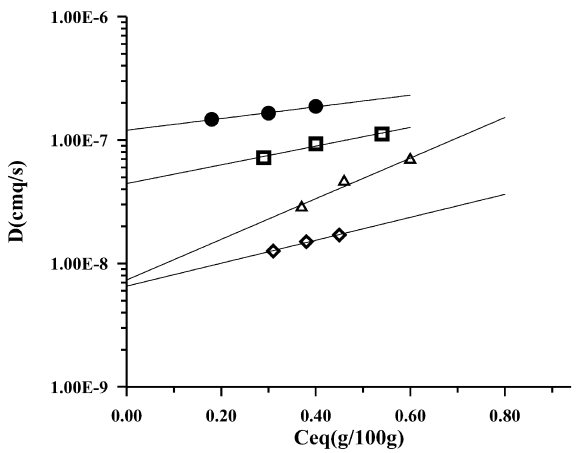

Fig. 6. Diffusion coefficient, D (cm^2/s), of water vapor as function of C_{eq} (g/100 g) for samples NPU0 (●), NPU4 (□), NPU20 (△), NPU40 (◇).

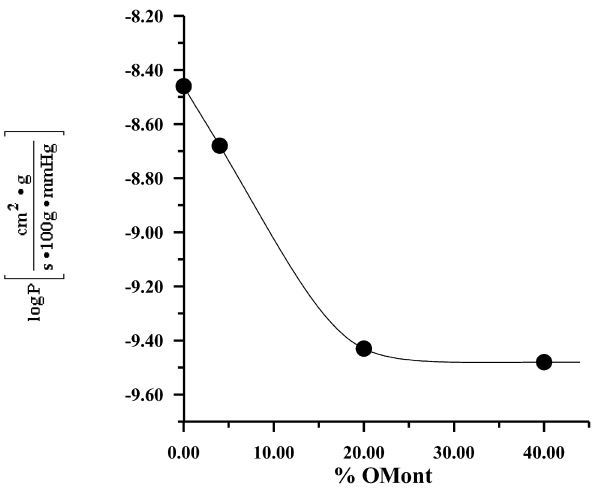

Fig. 7. Log of permeability (P) of all the samples to the water vapor at 30 °C as a function of OMont content.

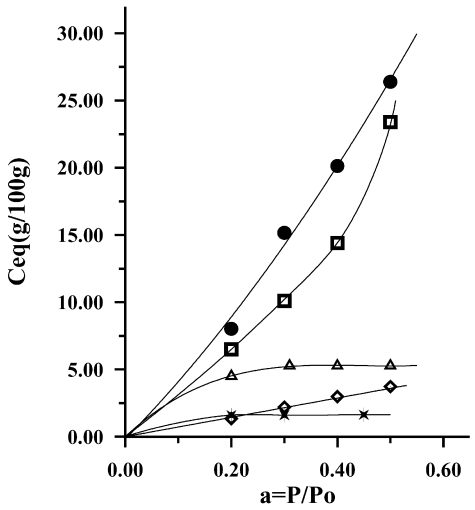

Fig. 8. Equilibrium concentration of dichloromethane vapor, C_{eq}, as a function of activity $a = p/p_0$ for samples OMont (★), NPU0 (●), NPU4 (□), NPU20 (△), NPU40 (◇).

plasticizing effect of the solvent into the polymer is more pronounced, as confirmed by a more than a linear increase in sorption with the vapor activity. The trend is quite different in the case of the samples with higher OMont content. The higher is the OMont content the more glassy appears the system, and no plasticizing effect of the solvent is observed [33]. The values of sorbed solvent decreases with increasing OMont over the whole investigated activity range. Also in this case it is possible to derive the sorption coefficient calculating the slope of the straight line at $a \leq 0.2$ in the C_{eq} versus p curve; the S parameters are reported in Table 5.

To derive the D_0 parameter, in Fig. 9 the diffusion coefficients as a function of the equilibrium concentration of dichloromethane vapor absorbed by the samples are reported. The plot can be analyzed in two different ranges: at low vapor concentrations, corresponding to low activities, the diffusion parameter is linearly dependent on the equilibrium concentration. For higher vapor activities, the

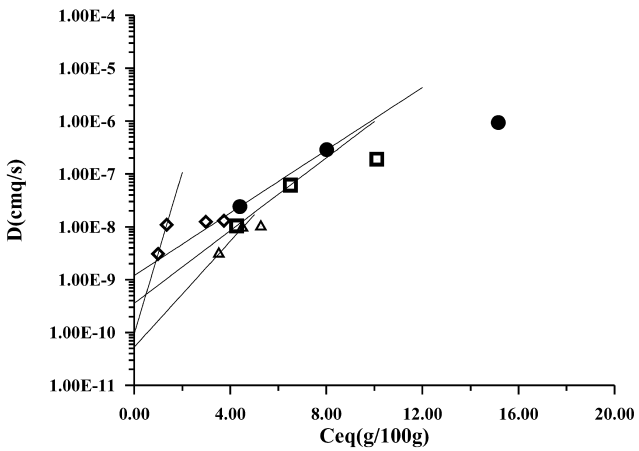

Fig. 9. Diffusion coefficient, D (cm^2/s), of dichloromethane vapor as function of C_{eq} (g/100 g) for samples NPU0 (●), NPU4 (□), NPU20 (△), NPU40 (◇).

Table 5
Zero-concentration diffusion coefficients, D_0 (cm^2/s), and sorptions S (g/100 g mm Hg) of dichloromethane vapor at $a \leq 0.2$ for all the analyzed samples

Sample	S[a] (g/100 g mm Hg)	$D_0 \times 10^9$ (cm^2/s)
PU	0.098	1.19
NPU4	0.079	0.355
NPU20	0.055	0.0529
NPU40	0.016	0.0941

[a] Evaluated as the slope of the straight line at $a \leq 0.2$ in the C_{eq} versus p (in mm Hg) curve.

vapor concentrations is able to completely plasticize the polymer, leading to a high mobility of polymer chains that can determine a transition in the diffusion–concentration curve. This transition is manifested by the curvature that occurs at higher concentrations, leading to very similar diffusion coefficients for the different samples. To extrapolate to zero penetrant concentration and obtain the D_0 parameters, we used only the values derived at low vapor activities. The values of D_0 are reported for all the samples in Table 5. The logarithm of permeability of the nanocomposites to dichloromethane as a function of the OMont content in NPUs is shown in Fig. 10. As already observed for the water vapor, a higher content of OMont in the hybrids gives rise to a lower values of the permeability, and the improvement of the barrier properties, also in this case, is significant up to 20% of OMont.

4. Conclusions

Samples of PU and OMont were prepared using, as soft segments, poly(ε-caprolactone)–OMont nanocomposites in a wide range of clay composition, between 4 and 40 wt%.

The X-ray analysis showed that exfoliation occurred for

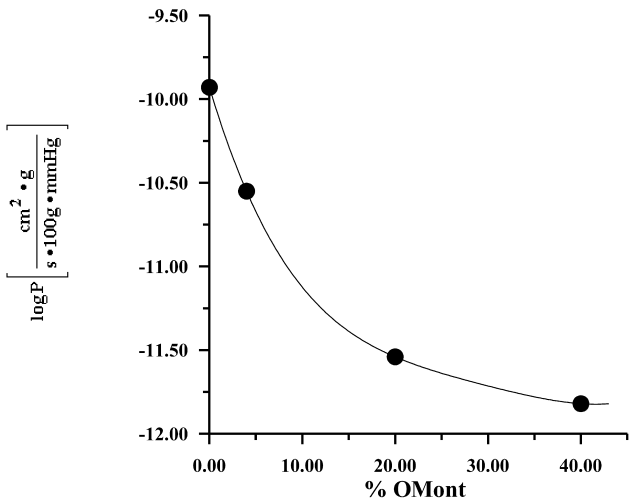

Fig. 10. Log of permeability P of all the samples to the dichloromethane vapor at 25 °C as a function of OMont content.

low montmorillonite content, whereas for higher contents the intercalated clay rearranged to a minor extent.

However, either exfoliated or delaminated samples showed an improvement in the elastic modulus and yield stress but a decrease in the stress and strain at breaking on increasing the clay content. In the case of high inorganic content, the melting of the poly(ε-caprolactone) crystalline regions did not determine the loss of mechanical consistence of the sample indicating that a network structure is formed.

Transport properties, measured for two different vapors, showed that the sorption did not drastically change on increasing the clay content, whereas the zero-concentration diffusion parameter (D_0) strongly decreased on increasing the inorganic content. The permeability, calculated as the product SD_0, showed a remarkable decrease up to 20% of clay and a leveling off at higher contents. It was largely dominated by the diffusion parameter.

Acknowledgements

This work was carried out with financial support from the Italian Ministry of the University and Scientific Research. The authors also thank Laviosa Chimica Mineraria SpA (Livorno, Italy) for kindly supplying the montmorillonite mineral.

References

[1] Komarneni SJ. J Mater Chem 1992;2:1219.
[2] Giannelis EP. Adv Mater 1996;8:29.
[3] Ziolo RF, Giannelis EP, Weinstein BA, O'Horo MP, Granguly BN, Mehrota V, Russell MW, Hoffman DR. Science 1992;257:219.
[4] Alexandre M, Dubois P. Mater Sci Engng 2000;28:1.
[5] Yano K, Usuki A, Okada A, Kurauchi T, Kamigaito O. J Polym Sci, Part A: Polym Chem Ed 1993;31:2493.
[6] Moet AS, Akelah A. Mater Lett 1993;18:97.
[7] Meier LP, Shelden RA, Caseri WR, Suter UW. Macromolecules 1994; 27:1637.
[8] Noh MW, Lee DC. Polym Bull 1999;42:619.
[9] Dietsche F, Müllaupt R. Polym Bull 1999;43:395.
[10] Fisher HR, Gielgens LH, Koster TPM. Acta Polym 1999;50:122.
[11] Liu L, Qi Z, Zhu X. J Appl Polym Sci 1999;71:1133.
[12] Reichert P, Hansjörg N, Klinke S, Brandsch R, Thomann R, Mülhaupt R. Macromol Mater Engng 2000;275:8.
[13] Vaia RA, Giannelis EP. Polym Commun 2001;42:1281.
[14] Kaempfer D, Thomann R, Mülhaupt R. Polymer 2002;43:2909.
[15] Chen TK, Tien YI, Wei KH. J Polym Sci, Part A: Polym Chem 1999; 37:2225.
[16] Sanders KJ. Organic polymer chemistry, 2nd ed. London: Chapman & Hall; 1988. p. 358.
[17] Hepburn C, Reynolds RJW. In: Ledwith A, North AM, editors. Molecular behaviour and development of polymeric materials. London: Chapman & Hall; 1974. p. 238.
[18] Backus JK. Encyclopedia of polymer science and engineering, vol. 13, Wiley-Interscience, N.Y. 1988, p. 243.
[19] Wang CB, Cooper SL. Macromolecules 1983;16:775.
[20] Li F, Hou J, Zhu W, Zhang X, Xu M, Luo X, Ma D, Kim BK. J Appl Polym Sci 1996;62:631.
[21] Li F, Zhang X, Hou J, Xu M, Luo X, Ma D, Kim BK. J Appl Polym Sci 1997;63:1511.
[22] Cooper SL, Tobolsky AV. J Appl Polym Sci 1966;10:1837.
[23] Lagasse RR. J Appl Polym Sci 1977;21:2489.
[24] Seefried CG, Koleske JV, Critchfield FE. J Appl Polym Sci 1975;19: 2493.
[25] Seefried CG, Koleske JV, Critchfield FE. J Appl Polym Sci 1975;19: 2503.
[26] Seefried CG, Koleske JV, Critchfield FE. J Appl Polym Sci 1975;19: 3185.
[27] Wang CB, Cooper SL. Macromolecules 1983;16:775.
[28] Tortora M, Vittoria V, Galli G, Ritrovati S, Chiellini E. Macromol Mater Engng 2002;287:243.
[29] Kajiyama T, MacKnight WJ. Trans Soc Rheol 1969;13:527.
[30] Gorrasi G, Tortora M, Vittoria V, Galli G, Chiellini E. J Polym Sci, Part B: Polym Phys 2002;40:1118.
[31] Bove L, D'Aniello C, Gorrasi G, Guadagno L, Vittoria V. J Appl Polym Sci 1996;62:1035.
[32] Barra G, D'Aniello C, Guadagno L, Vittoria V. J Mater Sci 1999;34: 4601.
[33] Rogers CE. Physics and chemistry of organic solid state. New York: Interscience Publisher; 1965.